

# Controlled propulsion and separation of helical particles at the nanoscale

Maria Michiko T. Alcanzare<sup>\*1</sup>, Vaibhav Thakore<sup>1</sup>, Santtu T. T. Ollila<sup>2</sup>, Mikko Karttunen<sup>3</sup>, and Tapio Ala-Nissila<sup>1,4</sup>

<sup>1</sup>COMP CoE at the Department of Applied Physics, Aalto University School of Science, P.O. Box 11000, FIN-00076 Aalto, Espoo, Finland

<sup>2</sup>Varian Medical Systems Finland, Paciuksenkatu 21, 00270 Helsinki, Finland

<sup>3</sup>Department of Mathematics and Computer Science & Institute for Complex Molecular Systems, Eindhoven University of Technology, P.O.Box 513, MetaForum 5600 MB Netherlands

<sup>4</sup>Department of Physics, Brown University, Providence, Rhode Island 02912-1843, USA

March 4, 2016

## Abstract

Controlling the motion of nano and microscale objects in a fluid environment is a key factor in designing optimized tiny machines that perform mechanical tasks such as transport of drugs or genetic material in cells, fluid mixing to accelerate chemical reactions, and cargo transport in microfluidic chips. Directed motion is made possible by the coupled translational and rotational motion of asymmetric particles. A current challenge in achieving directed and controlled motion at the nanoscale lies in overcoming random Brownian motion due to thermal fluctuations in the fluid. We demonstrate that controlled propulsion of nanohelices in an aqueous environment is possible using full-scale hydrodynamic simulations. We optimize the propulsion velocity and the efficiency of externally driven nanohelices. We quantify the importance of the thermal effects on the directed motion by calculating the Péclet number for various shapes, number of turns and pitch lengths of the helices. Consistent with the experimental microscale separation of chiral objects, our results indicate a chiral separation of nanohelices at Péclet numbers  $> 10$ . In addition, we find that the optimal fluid viscosity for the maximal efficiency of rotational motion in propelling a helical nanoparticle is  $\approx 3.5 \times 10^{-3}$  Pa s, close to the typical viscosity of blood. Our results provide criteria for the design and control of helical machines at the nanoscale.

Most natural organisms and molecules exhibit chiral structures that significantly influence their chemical and physical behavior. For example, most proteins are left-handed while sugars are right-handed. Drug molecules which target proteins, therefore, have different effects depending on their

---

<sup>\*</sup>maria.alcanzare@aalto.fi

chirality. Thalidomide is perhaps the most infamous example of a drug whose devastating health effects have been ascribed to the presence of both left and right handed enantiomers [6]. Motion and kinetics of chiral objects are largely determined by their spatial anisotropy since it leads to a coupling between the translational and rotational (TR) degrees of freedom. In biological systems, TR coupling is utilized by microorganisms that propel themselves in fluids by rotating their flagella and generating a chirality.

Artificially manufactured chiral particles with coupled TR motion provide many opportunities for technological applications [29, 8, 28, 27, 4, 15]. Recently, Clemens *et al.* have experimentally demonstrated separation of racemic mixtures by exposing left and right-handed chiral molecules to a rotating electric field. The dipole moments of the molecules in the racemic mixture align with the rotating electric field leading to their rotational motion. This propels the chiral molecules via the TR coupling and gives rise to enantiomer separation depending on their handedness [2]. Controlled and directed motion of chiral particles has important applications in targeted delivery of genetic material and drugs, too, because such particles can be tailored to facilitate their efficient uptake by various cells or tissues [25]. Tottori *et al.* demonstrated controlled motion and cargo transport of magnetic helical particles [28]. Application of time-dependent magnetic fields on magnetic screw-like particles induces a torque that rotates the particle and propels it in the fluid. Manipulation of the direction of the rotating magnetic fields makes it possible to load microspheres as cargo into the holder of a helical particle, transport the cargo and then release it at a preferred site [28]. Medina-Sánchez *et al.* have even demonstrated the possibility of assisted sperm delivery on immotile live sperm using externally driven microhelices [15]. Walker *et al.*, on the other hand, focused on optimizing the propulsion velocity of helices with a payload by varying the helical length [29]. In the experiments above, the propellers are typically 200 – 300 nm wide and 1 – 2  $\mu\text{m}$  long [29, 8, 28, 27].

On the theoretical side, exact analytic results for the drag coefficients of a certain high-symmetry shapes, such as spheres and ellipsoids can be obtained in the Stokes limit. For more complex shapes such as chiral particles, the boundary integral formulation of the Stokes equation can be used [12, 8, 30]. The resistive force theory (RFT) calculates propulsion velocity by summing the drag and thrust contributions of each infinitesimal segment of a rotating helical particle [3, 21]. Using a low Reynolds number approximation, the tangential and parallel components of the forces acting on an infinitesimal segment in the rigid body are assumed to be proportional to the tangential and parallel components of its velocity [3]. The main weakness lies in the neglect of the hydrodynamic interactions from fluid flows due to the other parts of the helical body. An improved low Reynolds number analysis incorporates these hydrodynamic interactions by discretizing the flagella into Stokeslets located at the cross-sectional centers of the helical particle and calculating the response of each Stokeslet due to the other segments of the body [22, 10]. However, with these analyses, the influence of the cross-sectional shapes of the helical particles cannot be explored.

Recently, artificial helical particles at the nanoscale with radii less than 100 nm have become available [26, 9, 5, 23]. Controlled propulsion has been experimentally demonstrated in a biological gel and in a high viscosity glycerol-water mixture (25 cP) but at low viscosities such as pure water, Brownian motion was greater than the propulsion of the nanohelix such that no directed motion was observed [23]. The challenge in controlling nanohelices is overcoming thermal effects which can significantly change the direction of motion and hinder the propulsion hence their coupled TR motion in aqueous solutions have not been characterized yet. Open questions include how the chiral geometry and the fluid properties affect the efficiency and the propulsion speed in cargo delivery. Here, we address these issues by employing the recently developed fluctuating Lattice-

Boltzmann - Molecular Dynamics (LBMD) method [17, 18, 13, 14, 19]. The method incorporates full Navier-Stokes hydrodynamics with consistent thermal fluctuations and a coupling of the fluid to extended MD particles of arbitrary shapes. We consider externally driven helices with radii of 30 nm, optimize the shape parameters and identify the conditions for controlled and directed motion, and chiral separation of helices at the nanoscale in general. Our results provide clear criteria for the physical parameters such as the Péclet number and fluid viscosity essential to studying applications of driven helical particles in nanoscale systems.

## Results

### Shape optimization of the helical particles

The fundamental quantity to be considered in the driven motion of helical particles is the propulsion velocity  $v$  induced by applying a constant external torque. We first present results for optimizing the geometric shape parameters for the helical particles shown in Fig. 1 such that  $v$  is maximized by using Method 1 as described in the Methods section. During optimization the hydrodynamic interactions are fully taken into account, but thermal noise is neglected.

The velocity  $v$  depends on several parameters. The drag force experienced by a helical particle as it propels in the fluid depends on the shape of its cross-section. We consider here three different shapes as shown in Fig. 6, where the helix has a circular cross-section and helicoids A and B have elliptic cross-sections. The helicoid A (B) has its long axis parallel (perpendicular) to the radial direction of the long axis. The volumes of the helical particles are kept constant here and the elliptic cross-sections of helicoids A and B have a linear eccentricity of  $\sqrt{3}/2$ . Other relevant parameters are the number of helical turns  $N$  and the pitch length (defined as the length  $L$  for one full turn of a helix). We keep the helical radius fixed at  $R = 30$  nm and thus optimize the ratio  $L/R$ . In the shape optimization a fluid density and viscosity of water at room temperature are used as  $\rho = 998$  kg/m<sup>3</sup> and  $\eta = 1.0$  mPa s, respectively.

Comparing the different helical particles in Fig. 1 we find that for all the pitch lengths considered, the angular velocity of the helix is the highest of them all (cf. SI Fig. ??) because it displaces the least fluid during rotation. Also, the helix yields the greatest propulsion velocity when the pitch length is varied, as shown in Fig. 2.a because it has the smallest circular area of cross-section resulting in the lowest drag along the long axis. The maximum propulsion velocity for the helix is obtained around  $L/R \approx 6$  (Fig. 2.a) for  $N = 1.25$ . As shown in SI Fig. ??, due to the strong spatial asymmetry of the helices there is significant wobbling for  $N < 1.125$ . In order to achieve maximum propulsion, both wobbling and the drag force must be minimized, and thus  $N$  must be larger than unity. In Fig. 2.b we show the propulsion velocity for two values of  $L/R$  in the region of the velocity maximum as a function of  $N$ , showing that the optimal number of turns is indeed  $N \approx 1.25$ . This is consistent with the experimental result of Walker *et al.* [29], where maximum propulsion is achieved for about one full helical turn for micron sized particles.

### Propulsion efficiency

In addition to maximizing the propulsion velocity, it is also useful to characterize the efficiency of the helix. The dynamics at the low Reynolds number of a particle is described by the generalized

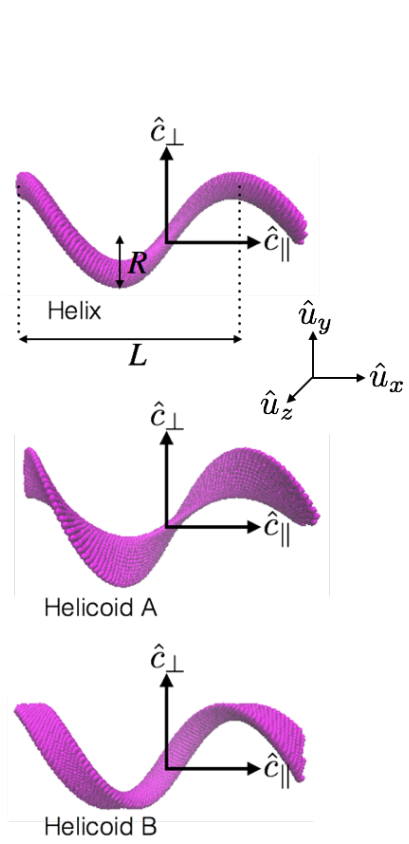


Figure 1: **Geometry of the helical particles.** Shapes of different helices with a helical radius of  $R$ , helical turns  $N = 1.25$  and pitch length  $L$ . The unit vectors  $\hat{u}_x$ ,  $\hat{u}_y$  and  $\hat{u}_z$  represent coordinates in the laboratory frame, while  $\hat{c}_\perp$  and  $\hat{c}_\parallel$  represent the coordinates in the body frame of the helical particles.

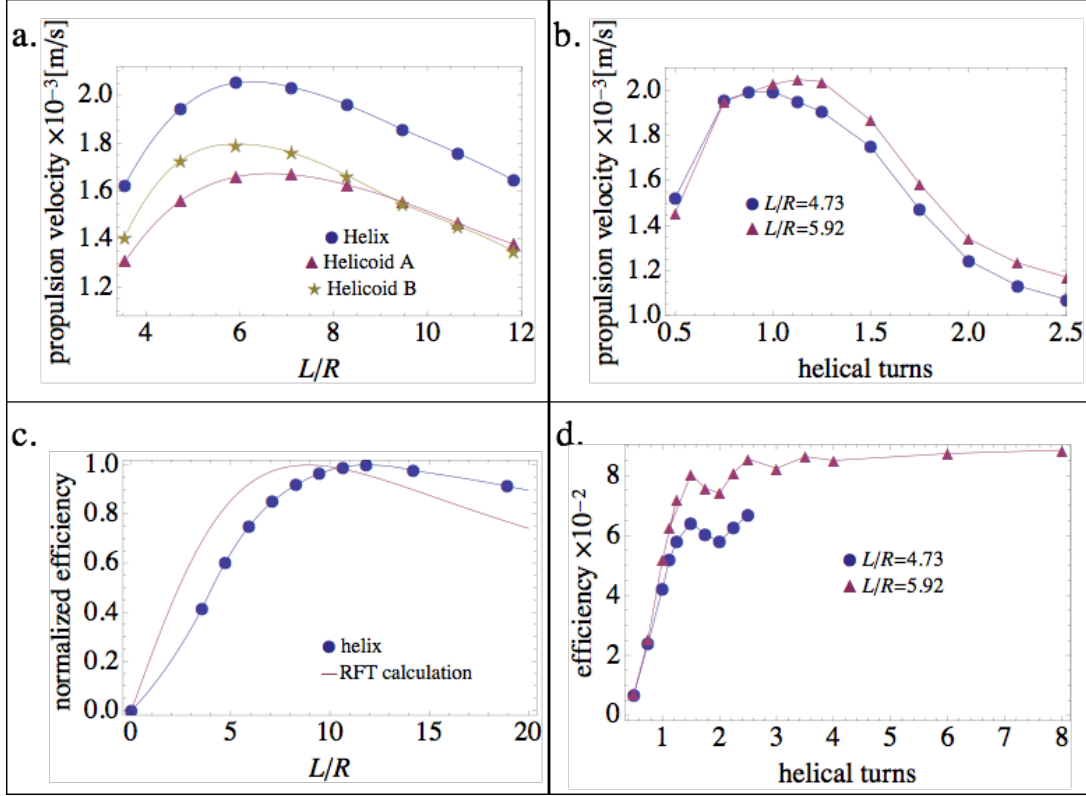


Figure 2: **Optimization of the helical particles.** a. Propulsion velocities as a function of  $L/R$  of the helix, helicoid A, and helicoid B for  $N = 1.25$  with a constant torque of  $1.0 \times 10^{-18}$  kg  $\text{m}^2/\text{s}^2$ .  $L/R \approx 6$  results in maximum propulsion velocities for the helix, and helicoids A and B. b. Propulsion velocities as a function of the number of helical turns of a helix with  $L/R = 4.73$  and  $L/R = 5.92$ . The applied constant torque is  $1.0 \times 10^{-18}$  kg  $\text{m}^2/\text{s}^2$ . c. Normalized efficiency of a helix with  $N = 1.25$  and the efficiency of a low Reynolds number RFT calculation from Ref. [3] as a function of  $L/R$ . d. Efficiency  $\epsilon \equiv v/(\omega R)$  of helices of pitch length and radius ratio of 4.73 and 5.92.

resistance tensor

$$\begin{pmatrix} \mathbf{F} \\ \boldsymbol{\tau} \end{pmatrix} = \begin{pmatrix} \boldsymbol{\xi}^{\text{TT}} & \boldsymbol{\xi}^{\text{TR}} \\ \boldsymbol{\xi}^{\text{RT}} & \boldsymbol{\xi}^{\text{RR}} \end{pmatrix} \begin{pmatrix} \mathbf{v} \\ \boldsymbol{\omega} \end{pmatrix}, \quad (1)$$

where  $\mathbf{F}, \boldsymbol{\tau}, \mathbf{v}, \boldsymbol{\omega}$  and  $\boldsymbol{\xi}^{\alpha\beta}$  are the net force, torque, translational velocity, angular velocity and the friction matrix of the particle, respectively [20]. Particles with spherical symmetry have zero non-diagonal terms in the friction matrix and diagonal terms correspond to the Stokes translational and rotational drag coefficients. For a helix, when a torque is applied along its long axis, the rotational motion drives it forward along this same axis through the non-zero coupling term  $\boldsymbol{\xi}^{\text{TR}}$  or  $\boldsymbol{\xi}^{\text{RT}}$ . To characterize the TR coupling, we define the efficiency  $\epsilon$  to be the constant of proportionality of the propulsion velocity and the angular velocity,  $\epsilon \equiv v/(\omega R)$ , where  $R$  is the helical radius.

Within the resistive force theory (RFT), there exists an approximate analytic result for the (relative) efficiency given by

$$\epsilon' = \frac{\sin 2\theta}{3 - \cos 2\theta} \quad (2)$$

where  $\theta$  is the pitch angle that is related to the pitch length and the helical radius by  $\tan \theta = 2\pi R/L$  [3, 21]. In Fig. 2.c. we compare the numerically obtained results for the efficiency of a helix ( $N = 1.25$ ) to that in Eq. (2), normalized by their maximum values.<sup>1</sup> In our data, the maximum efficiency is achieved at  $L/R \approx 11.7$ , which is about 1.3 times larger than that predicted by Eq. (2).

In Fig. 2.d. we show numerical results for the efficiency as a function of the number of turns  $N$  for two values of  $L/R$  close to the optimum in Fig. 2.a. In contrast to Eq. (2), where there is no  $N$  dependence, with full hydrodynamics we find nontrivial dependence of  $\epsilon$  on  $N$ . The stability of the rotational motion and propulsion, and consequently the efficiency, increases with the number of turns from  $N = 0.5$  to  $N = 1.5$ , where there is a local maximum. Beyond  $N = 1.25$ , the efficiency exhibits damped oscillations before saturating to a constant value, where both  $\omega$  and  $v$  asymptotically decrease as  $N^{-1}$  (see SI Fig. ?? and Fig. 1.2.b).

Experimentally, the propulsion of some polarly flagellated organisms has been observed to depend on fluid viscosity [24, 1], and thus we have also varied  $\eta$  in our simulations. Consistent with the predictions in the Stokes limit, we find that both the angular velocity and the propulsion velocity vary  $\propto 1/\eta$  in the limit of high fluidity (see SI Fig. ??). In Fig. 3 we show  $\epsilon$  as a function of fluidity ( $1/\eta$ ) for viscosities in the range  $(0.75 - 9) \times 10^{-3}$  Pa s. The trend in the efficiency as a function of fluidity is similar to that of flagellated bacteria in references [24, 1]. This is despite the fact that the bacteria can adjust their shapes in response to viscosity changes. Perhaps the most striking result in Fig. 3 is the existence of a maximum in  $\epsilon$  at  $\eta \approx 3.5 \times 10^{-3}$  Pa s, close to the viscosity of blood. It should be noted, however, that the variation in efficiencies at different fluidities is relatively small, only about 3.5%.

## Influence of thermal fluctuations

### Directed motion and chiral separation

For directed motion of the helical particles, the Péclet number ( $\text{Pe} \equiv vL/D_T$ , where  $D_T$  is the Brownian tracer diffusion coefficient of the particle) quantifies the strength of the propulsive versus

---

<sup>1</sup>For the efficiencies of different shapes see SI Fig. ??.

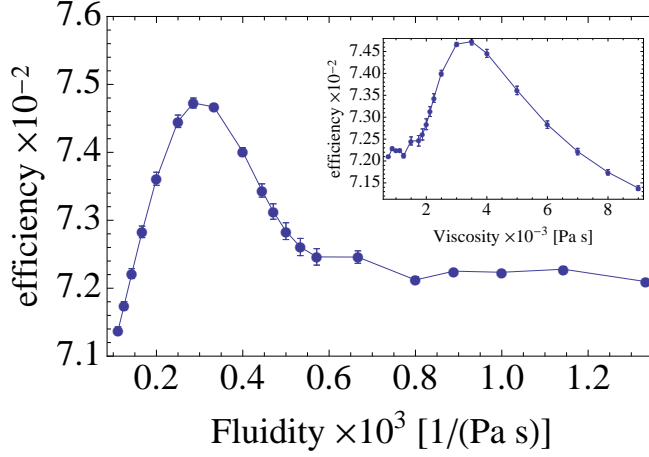


Figure 3: **Fluidity dependence of the propulsion.** Efficiency of a helix with  $L/R = 5.92$  and  $N = 1.25$  as a function of the fluidity ( $1/\eta$ ). Maximum efficiency is achieved at  $\eta \approx 3.5 \times 10^{-3}$  Pa s. Inset shows the same data as a function of  $\eta$ .

random diffusive motion and is thus a relevant measure of thermal fluctuations. It can be written as

$$\text{Pe}(\omega) = \frac{6\pi\eta R_H}{k_B T} \epsilon \omega R L, \quad (3)$$

where  $R_H$  is the effective size (hydrodynamic radius) of the particle. As can be seen from Eq. (3), the effect of temperature is typically negligible for micron size particles due to the large  $\text{Pe}$  for relevant velocities, and has not been considered to date. However, at the nanoscale  $\text{Pe}$  is not necessarily large and thermal fluctuations need to be fully accounted for. To model the experiments where magnetic helices were driven by an external field [29, 8, 28, 4, 15], we have used Method 2 with thermal fluctuations (Methods section) and simulated the particle motion in water at 300 K.

In the Supplementary (SI Fig. ??) we show how  $D_T$  depends on  $N$ . As expected,  $\text{Pe}$  grows linearly with the applied torque (SI Fig. ??a). To obtain directed motion,  $N$  must be greater than unity to minimize wobbling. In Fig. 4 we present data for the propulsion velocity of an optimal nanohelix ( $N = 1.25$ ,  $R = 30$  nm and  $L/R = 5.92$ ) as a function of the external torque with and without thermal fluctuations. From the data we can conclude that directed motion becomes very well established for Péclet numbers greater than approximately 50.

Separation of magnetic helical colloids with a radius  $R \approx 0.3 \mu\text{m}$  and number of turns  $N = 5$  has been experimentally demonstrated at high ratios ( $\sim 10^3$ ) of torque strengths and thermal energies [4]. Next, we present results for magnetic nanoscale helices ( $R = 30$  nm and  $L/R = 5.92$ ) with positive (+) and negative (−) helicities using Method 2 with thermal fluctuations at 300 K.

In the absence of an external magnetic field no torque is exerted on the magnetic nanohelices and purely diffusive motion is observed. We denote  $\tau_{\text{max}}$  as the product of the magnetization and the magnetic field. For  $\tau_{\text{max}} > 0$  and in the absence of thermal fluctuations, chiral particles with (+) and (−) helicities move in the two opposite directions parallel to their long axis. In Fig. 5a, we show typical displacement trajectories of the (+) and (−) helices with 0.5 and 1.25 helical turns for various torque strengths. At  $\tau_{\text{max}} = 1.0 \times 10^{-19}$  kg m<sup>2</sup>/s<sup>2</sup>, the angular velocity obtained is

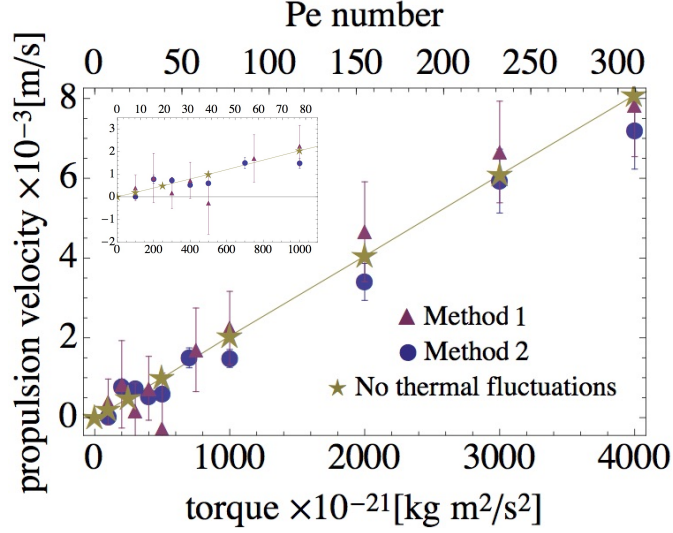


Figure 4: **Propulsion velocities at various torque strengths.** Average propulsion velocities for varying torque strength of a helix with  $N = 1.25$  helical turns and  $L/R = 5.92$  in simulations without thermal fluctuations, and with thermal fluctuations using either Method 1 or 2. Inset shows details of the data for the small Pe number regime.

not sufficient to separate the chiral particles with  $N = 0.5$  and  $N = 1.25$ . At a higher torque  $\tau_{\max} = 2.0 \times 10^{-19}$  kg m<sup>2</sup>/s<sup>2</sup>, the longer helical particles ( $N = 1.25$ ) get separated while chiral separation for the short particles is still not possible. In general, we conclude that Péclet numbers below about 10 are definitely not sufficient to separate chiral particles. This result is consistent with the experimentally demonstrated chiral separation of microscale bacteria in sheared flows [7].

## Summary and Conclusions

We have shown here that helical particles with a circular cross-section characterized by a minimum surface area result in optimal propulsion in terms of maximising the propulsion velocity. A circular cross-section of the flagella, often naturally encountered in many organisms, is thus optimized for propulsion. Controlled propulsion in the presence of thermal fluctuations requires stability in the rotational motion (*i.e.*, minimum wobbling) which increases with the number of turns  $N$ . However, increase in the length adds to the hydrodynamic drag. Therefore, maximum propulsion is achieved by balancing the competing requirements for maintaining the stability of the rotational motion and minimizing viscous drag. Thus, the optimal number of turns,  $N = 1.25$ , required for obtaining maximum propulsion velocities in the high Péclet number limit reported here, is consistent with the previously published experimental results for microscale helices [29]. Furthermore, our results show that the fluid viscosity plays an important role in the efficiency of the coupled TR motion for externally driven helical nanopropellers. The computed fluid viscosity that results in maximum efficiency is seen to almost coincide with the typical viscosity for blood. At the nanoscale where thermal effects are significant, we have shown that for well-defined directed motion and chiral



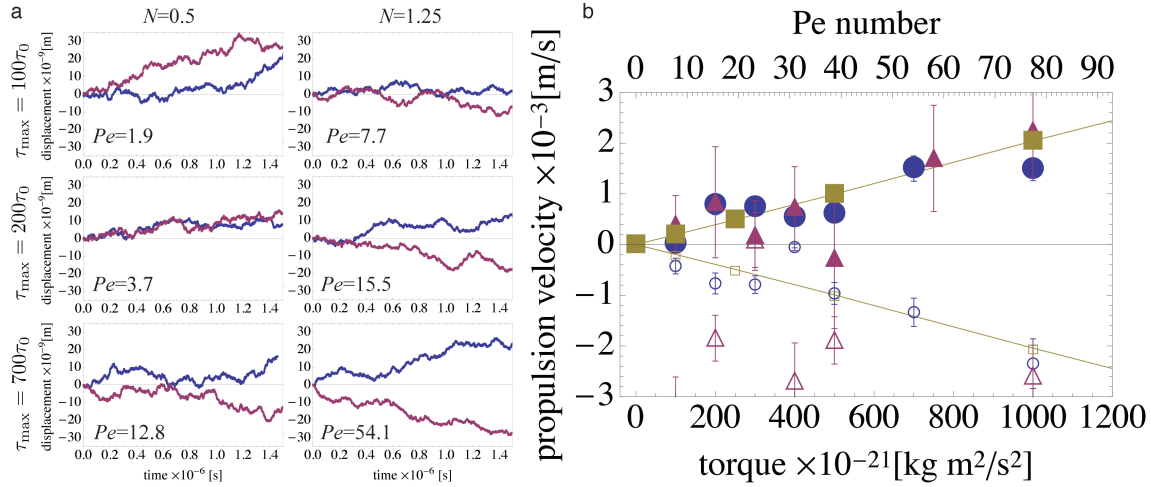


Figure 5: **Chiral separation.** a. Typical displacement trajectories vs. time of a positive (blue) and a negative (red) helix with a pitch length and helical radius ratio of  $L/R = 5.92$  that is driven by various torque strengths in the presence of thermal fluctuations using Method 2, with a maximum torque of  $\tau_{\max}$  ( $\tau_0 = 10^{-21}$  kg m<sup>2</sup>/s<sup>2</sup>). b. Measured average propulsion velocities of helices with  $N = 1.25$  helical turns and  $L/R = 5.92$  with thermal fluctuations using Method 1 (triangles), Method 2 (circles) and without thermal fluctuations (squares). Filled (empty) markers have positive (negative) chirality.

separation of magnetic particles, the Péclet number should definitely be larger than 10, in good agreement with the experiments on the chiral separation of microscale objects reported earlier [7].

## Methods

### Hybrid Lattice-Boltzmann - Molecular Dynamics method

The multiscale hybrid Lattice-Boltzmann - Molecular Dynamics (LBMD) method implemented in LAMMPS is used in simulating the propulsion of the helical nanoparticles in the fluid [17, 18, 13, 14, 19]. The method incorporates full Navier-Stokes hydrodynamics with consistent coupling of the MD particles to thermal fluctuations in the fluid.

We use physically extended helical nanoparticles. They are represented as composite particles with surface nodes that are treated as MD particles. The nodes are equally distributed on the surface with the center line following the parametric equation  $(R \cos t, R \sin t, tL/(2\pi))$ . The cross-sectional shape is given by  $R/4(a_1 \cos \phi, a_2 \sin \phi)$  where  $\phi \in [0, 2\pi)$  and  $a_1 = a_2 = 1$  for the helix,  $a_1 = 1/2$  and  $a_2 = 2$  for helicoids A and B. Helicoid A (B) has a long axis parallel (perpendicular) to the radial direction along the long axis. The node masses are set such that the total mass of the helix is equivalent to the mass of the displaced fluid and the area per node is given by 18.5 nm<sup>2</sup>.

The surface nodes interact with the fluid through an energy and momentum conserving interaction mediated through elastic collisions [17, 13]. The node and the fluid velocities after the elastic

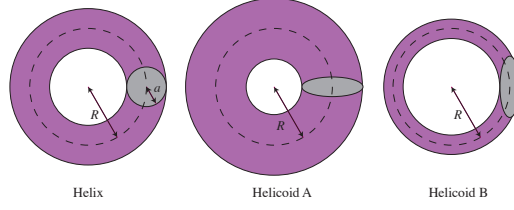


Figure 6: **Cross-sections of the helical particles.**

collision are given by

$$\mathbf{u}_f = \mathbf{u}_i + (\mathbf{v}_i - \mathbf{u}_i) \frac{2m_v}{m_v + m_u}, \quad (4)$$

$$\mathbf{v}_f = \mathbf{v}_i - (\mathbf{v}_i - \mathbf{u}_i) \frac{2m_u}{m_v + m_u}, \quad (5)$$

where  $m_v$  and  $m_u$  ( $\mathbf{v}$  and  $\mathbf{u}$ ) are the node and fluid mass (velocity), respectively [13]. An explicit no-slip boundary condition at the fluid-particle interface is implemented in all the simulations. This boundary condition sets the sum of the initial and the final relative fluid-node velocities to zero. All simulations are carried out with a lattice discretization of  $\Delta x = 13.245$  nm and  $\Delta t = 29.1859$  ps.

## Implementation of the external torque

The rotation of a helical particle in the simulations can be induced using two different methods. In the first method (Method 1), a constant torque is applied along the long axis of the helix. This corresponds to the synchronous high-frequency regime wherein the frequency of rotation of the helix matches the frequency of rotation of the external magnetic field that exerts a torque on it [16]. In the absence of thermal fluctuations, Method 1 is employed as a means to optimize the geometrical shape for the helical particle and the fluid viscosity that result in optimal propulsion and efficiency.

In the second method (Method 2), the motion of a magnetic helical particle is modeled in the presence of an externally applied rotating magnetic field. The torque experienced by the helical particle is given by  $\vec{\tau} = \vec{m} \times \vec{B}$ , where  $\vec{m}$  is the magnetization of the helical particle and  $\vec{B}$  is the external magnetic field given by  $\vec{B}(t) = B_0[\cos(\omega t)\hat{u}_y + \sin(\omega t)\hat{u}_z]$ . The magnetization is set such that it is parallel to  $\hat{c}_\perp$ . The initial orientation of the magnetization the helical particle is parallel to  $\vec{B}(0)$ . To minimize its energy, the particle aligns its magnetization with the direction of the rotating magnetic field  $\vec{B}$ . This induces a rotation in the helical particle. When the initial configuration of the long axis of the helical particle is aligned along the  $\hat{u}_x$  direction (see Fig. 1), the deviations in the orientation of the long axis from its initial configuration are minimal for both methods provided the Péclet number is large enough. Here we use  $\omega = 20$  MHz and denote the maximum torque,  $\tau_{\max}$ , as the product of the magnetization and the external magnetic field.

## Acknowledgements

This work was supported in part by the Academy of Finland through its Centres of Excellence Programme (2012-2017) under Project No. 251748 and Aalto Energy Efficiency Research Programme.

We acknowledge the computational resources provided by Aalto Science-IT project and CSC-IT. The graphical representation in the Fig. 1 were rendered using VMD [11].

## Competing financial interests

The authors declare no competing financial interests.

## References

- [1] ATSUMI, T., ET AL. Effect of viscosity on swimming by the lateral and polar flagella of vibrio alginolyticus. *Journal of Bacteriology* 178, 16 (1996), 5024–5026.
- [2] CLEMENS, J. B., KIBAR, O., AND CHACHISVILIS, M. A molecular propeller effect for chiral separation and analysis. *Nature communications* 6 (2015).
- [3] DE LIMA BERNARDO, B., AND MORAES, F. Simplified model for the dynamics of a helical flagellum. *American Journal of Physics* 79, 7 (2011), 736–740.
- [4] DEBORA, S., ET AL. Chiral colloidal molecules and observation of the propeller effect. *Journal of the American Chemical Society* 135, 33 (2013), 12353–12359.
- [5] ESLAMI, S., ET AL. Chiral nanomagnets. *Acs Photonics* 1, 11 (2014), 1231–1236.
- [6] FRANKS, M. E., MACPHERSON, G. R., AND FIGG, W. D. Thalidomide. *The Lancet* 363, 9423 (2004), 1802–1811.
- [7] FU, H. C., POWERS, T. R., STOCKER, R., ET AL. Separation of microscale chiral objects by shear flow. *Physical review letters* 102, 15 (2009), 158103.
- [8] GHOSH, A., AND FISCHER, P. Controlled propulsion of artificial magnetic nanostructured propellers. *Nano letters* 9, 6 (2009), 2243–2245.
- [9] GIBBS, J., MARK, A., ESLAMI, S., AND FISCHER, P. Plasmonic nanohelix metamaterials with tailorable giant circular dichroism. *Applied Physics Letters* 103, 21 (2013), 213101.
- [10] HANCOCK, G. J. The self-propulsion of microscopic organisms through liquids. *Proceedings of the Royal Society of London A: Mathematical, Physical and Engineering Sciences* 217, 1128 (1953), 96–121.
- [11] HUMPHREY, W., DALKE, A., AND SCHULTEN, K. Vmd: visual molecular dynamics. *Journal of molecular graphics* 14, 1 (1996), 33–38.
- [12] KEAVENY, E. E., WALKER, S. W., AND SHELLEY, M. J. Optimization of chiral structures for microscale propulsion. *Nano letters* 13, 2 (2013), 531–537.
- [13] MACKAY, F., AND DENNISTON, C. Coupling md particles to a lattice-boltzmann fluid through the use of conservative forces. *Journal of Computational Physics* 237 (2013), 289–298.

- [14] MACKAY, F., OLLILA, S., AND DENNISTON, C. Hydrodynamic forces implemented into lammmps through a lattice-boltzmann fluid. *Computer Physics Communications* 184, 8 (2013), 2021–2031.
- [15] MEDINA-SÁNCHEZ, M., SCHWARZ, L., MEYER, A., HEBENSTREIT, F., AND SCHMIDT, O. G. Cellular cargo delivery: Towards assisted fertilization by sperm-carrying micromotors. *Nano letters* (2015).
- [16] MOROZOV, K. I., AND LESHANSKY, A. M. The chiral magnetic nanomotors. *Nanoscale* 6, 3 (2014), 1580–1588.
- [17] OLLILA, S. T. T., DENNISTON, C., KARTTUNEN, M., AND ALA-NISSILA, T. Fluctuating lattice-Boltzmann model for complex fluids. *J. Chem. Phys.* 134, 6 (Feb. 2011), 064902.
- [18] OLLILA, S. T. T., SMITH, C., ALA-NISSILA, T., AND DENNISTON, C. The hydrodynamic radius of particles in the hybrid lattice boltzmann–molecular dynamics method. *Multiscale Model. Simul.* 11, 1 (2013), 213–243.
- [19] PLIMPTON, S. Fast parallel algorithms for short-range molecular dynamics. *J. Comput. Phys.* 117, 1 (1995), 1–19.
- [20] PURCELL, E. M. Life at low reynolds number. *Am. J. Phys* 45, 1 (1977), 3–11.
- [21] RAZ, O., AND AVRON, J. Swimming, pumping and gliding at low reynolds numbers. *New Journal of Physics* 9, 12 (2007), 437.
- [22] RODENBORN, B., CHEN, C., SWINNEY, H. L., LIU, B., AND ZHANG, H. P. Propulsion of microorganisms by a helical flagellum. *Proceedings of the National Academy of Sciences* 110, 5 (2013), E338–E347.
- [23] SCHAMEL, D., MARK, A. G., GIBBS, J. G., MIKSCH, C., MOROZOV, K. I., LESHANSKY, A. M., AND FISCHER, P. Nanopropellers and their actuation in complex viscoelastic media. *ACS nano* 8, 9 (2014), 8794–8801.
- [24] SCHNEIDER, W. R., AND DOETSCH, R. Effect of viscosity on bacterial motility. *Journal of Bacteriology* 117, 2 (1974), 696–701.
- [25] SINGH, R., AND LILLARD, J. W. Nanoparticle-based targeted drug delivery. *Experimental and molecular pathology* 86, 3 (2009), 215–223.
- [26] SONE, E. D., ZUBAREV, E. R., AND STUPP, S. I. Semiconductor nanohelices templated by supramolecular ribbons. *Angewandte Chemie International Edition* 41, 10 (2002), 1705–1709.
- [27] SUMIGAWA, T., ET AL. Substrate temperature control for the formation of metal nanohelices by glancing angle deposition. *Journal of Vacuum Science & Technology A* 33, 6 (2015), 060609.
- [28] TOTTORI, S., ET AL. Magnetic helical micromachines: fabrication, controlled swimming, and cargo transport. *Advanced materials* 24, 6 (2012), 811–816.
- [29] WALKER, D., KÜBLER, M., MOROZOV, K. I., FISCHER, P., AND LESHANSKY, A. M. Optimal length of low reynolds number nanopropellers. *Nano Letters* 15, 7 (2015), 4412–4416. PMID: 26030270.

- [30] ZHANG, L., ET AL. Artificial bacterial flagella: Fabrication and magnetic control. *Applied Physics Letters* 94, 6 (2009), 064107.